

# Organic & Biomolecular Chemistry

Accepted Manuscript



This is an *Accepted Manuscript*, which has been through the Royal Society of Chemistry peer review process and has been accepted for publication.

*Accepted Manuscripts* are published online shortly after acceptance, before technical editing, formatting and proof reading. Using this free service, authors can make their results available to the community, in citable form, before we publish the edited article. We will replace this *Accepted Manuscript* with the edited and formatted *Advance Article* as soon as it is available.

You can find more information about *Accepted Manuscripts* in the [Information for Authors](#).

Please note that technical editing may introduce minor changes to the text and/or graphics, which may alter content. The journal's standard [Terms & Conditions](#) and the [Ethical guidelines](#) still apply. In no event shall the Royal Society of Chemistry be held responsible for any errors or omissions in this *Accepted Manuscript* or any consequences arising from the use of any information it contains.

**Synthesis and Evaluation of A Novel Rhodamine B Pyrene [2]Rotaxane as an  
Intracellular Delivery Agent for doxorubicin**

Jiaxin Shi <sup>a, †</sup>, Yuan Xu <sup>b, †</sup>, Xinlong Wang <sup>d</sup>, Luyong Zhang <sup>b</sup>, Jing Zhu <sup>\*, c</sup>, Tao Pang  
<sup>\*, b</sup>, Xiaofeng Bao <sup>\*, a</sup>

<sup>a</sup> *Department of Biochemical Engineering, Nanjing University of Science and Technology, Chemical Engineering Building B308, 200 Xiaolingwei, Nanjing, 210094, P.R. China*

<sup>b</sup> *Jiangsu Key Laboratory of Drug Screening and State Key Laboratory of Natural Medicines, China Pharmaceutical University, Nanjing, 210009, P.R. China*

<sup>c</sup> *Department of Pharmacy, Nanjing University of Chinese Medicine, 138 Xianlin Dadao, Nanjing, 210023, P.R. China*

<sup>d</sup> *Department of Chemistry, School of Chemical Engineering, Nanjing University of Science & Technology, Nanjing, 210094, P.R. China*

\*Corresponding author: Dr. Xiaofeng Bao, E-mail: [baoxiaofeng@mail.njust.edu.cn](mailto:baoxiaofeng@mail.njust.edu.cn);

Dr. Tao Pang, E-mail: [tpang@cpu.edu.cn](mailto:tpang@cpu.edu.cn); Dr. Jing Zhu, Email:

[zhujing1227@hotmail.com](mailto:zhujing1227@hotmail.com)

<sup>†</sup> *These authors contributed equally to this work.*

**Abstract**

A novel Rhodamine B-derivatized host [2]rotaxane, containing a dibenzyl-24-crown-8 (DB24C8) ring as the wheel and a pyrene as another fluorophore blocking group, was designed, synthesized and structurally characterized. A comparison of the  $^1\text{H}$  NMR spectra of **RhBP**y [2]rotaxane with those of **2** and DB24C8, Nuclear Overhauser effect spectroscopy (NOESY), mass spectrometry and fluorescence spectroscopy confirmed the interlocked nature of **RhBP**y [2]rotaxane. The temperature dependence of the rotaxane studied by  $^1\text{H}$  NMR spectroscopy further demonstrated that **RhBP**y [2]rotaxane can be applied as a molecular switch. **RhBP**y [2]rotaxane has also been demonstrated to be an efficient transport agent for delivering the cancer drug doxorubicin (DOX) into tumor cells. Indeed, DOX delivered by **RhBP**y [2]rotaxane could effectively inhibit tumor cells' growth.

*Keywords: Rhodamine B, Rotaxane, Drug delivery, Doxorubicin, Cell imaging*

## Introduction

The design and development of drug delivery agents that can efficiently transport drugs into cells and release the drugs in a controlled fashion have attracted significant interest from chemists and biomaterial scientists because they offer the possibility of wide application in the medical field <sup>[1-5]</sup>. The difficulties associated with drug transporters are well exemplified in the development of synthetic transporters <sup>[6-9]</sup>. For a synthetic transporter to transport materials into cells, the transporter must recognize and form a complex with a targeted compound in the aqueous extracellular matrix, be attached to the negatively charged cell surface, stay bound to the compound through the highly apolar environment of a membrane, and release the compound within the cell or continue the transport process to a particular local, such as the nucleus <sup>[10-14]</sup>. For the transporter to act as an efficient cellular delivery agent, the transporter also needs to be soluble in these different environments on a level commensurate with the association constants of the host-guest complex <sup>[15-18]</sup>. Among many biologically important transport agents, rotaxanes, a class of interlocked supermolecules formed by threading cyclic molecules onto the axle chain with two blocking groups on the end to keep the wheel from dethreading, demonstrate not only unique structural features but also have a wide range of potential applications as molecular machines <sup>[19-20]</sup>, switches <sup>[21-23]</sup>, sensors <sup>[24-26]</sup> and artificial drug delivery agents <sup>[27-28]</sup>. Over the past decade, various macrocyclic molecules, such as cyclodextrins, crown ethers, and cucurbiturils, have been employed to construct rotaxanes <sup>[29-33]</sup>. Among them, crown ethers have attracted much attention due to their diverse binding selectivity. Although significant

efforts have been made to date, new and efficient methods for the synthesis of crown ether-based rotaxanes are still important and attractive <sup>[34-37]</sup>. We have previously demonstrated that host [2]rotaxanes <sup>[38-39]</sup> containing an arginine-derivatized dibenzyl-24-crown-8 (DB24C8) ring as the wheel and a cyclophane or cleft as a blocking group were a class of supermolecular compounds that could meet all cellular transporter requirements. The unique ability of the wheel to slide along the axle made rotaxanes a highly suitable choice as cellular transport agents. They can not only strongly associate with a variety of guests in DMSO, water, and mixed solvent systems with large association constants but can also act as intracellular transport agents to efficiently transport fluorescein and fluoresceinated peptides, such as FI-AVWAL, FI-QEAVD, and FI-KKALR, at sub-micromolar concentrations into the cytoplasm and nucleus of eukaryotic COS-7 cells. Although our previous studies have indicated that host [2]rotaxanes can bind and deliver fluorescein and fluoresceinated peptides into cells at concentration levels commensurate with association constants derived for the complexes formed in buffered water, DMSO and chloroform, the location of rotaxanes in cells has never been determined. To monitor the cellular permeability of rotaxane during the transport process and determine its cellular location, in this paper, a novel Rhodamine B-derivatized host [2]rotaxane containing a dibenzyl-24-crown-8 (DB24C8) ring as the wheel and a pyrene as another fluorophore blocking group (**Figure 1**) was designed, synthesized and structurally characterized. Rhodamine B and its derivatives have been extensively used both in biomolecular imaging and as fluorescent chemosensors for metal ions because of their

high absorption coefficients, high fluorescence quantum yields, and long absorption and emission wavelengths<sup>[40-43]</sup>. We considered that the novel Rhodamine B pyrene host [2]rotaxane would deliver materials as usual and that its drug delivery abilities could be determined by simply observing its red fluorescence in cells.

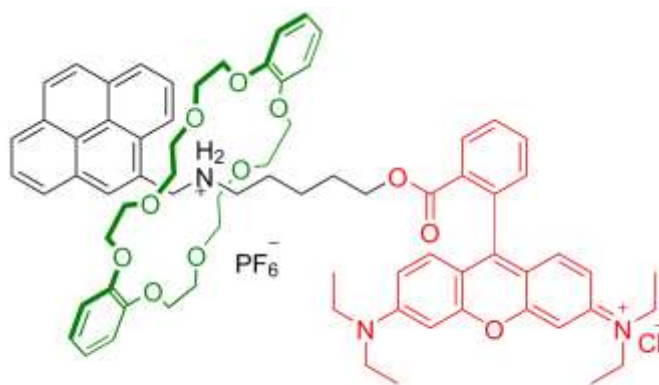


Figure 1. Chemical structure of the RhBPy [2]rotaxane

## Experimental

### Materials and general methods

All reagents and organic solvents used were of ACS grade or higher and were used without further purification. Unless otherwise noted, all chemicals were purchased from J&K Scientific (Shanghai, China) and were used as received. All solvents were of analytical grade, and double-distilled water was used in all experiments. Thin-layer chromatography was performed on a HAIYANG silica gel F254 plate, and compounds were visualized under UV light ( $\lambda = 254$  nm). Column chromatography was performed using HAIYANG silica gel (type: 200–300 mesh ZCX-2).  $^1\text{H}$  NMR (500 MHz) and  $^{13}\text{C}$  NMR (126 MHz) spectra were recorded on an Avance 500 spectrometer (Bruker; Billerica, MA, USA). Chemical shifts are reported in  $\delta$  units (ppm) downfield relative to the chemical shift of tetramethylsilane. The abbreviations br, s, d, t and m denote broad, singlet, doublet, triplet and multiplet, respectively.

Mass spectra were obtained with a Finnigan TSQ Quantum LC/MS spectrometer. High-resolution mass spectra (HRMS) were acquired under electron ionization conditions with a double-focusing high-resolution instrument (Autospec; Micromass Inc.) and an Edinburgh FLS920 fluorescence spectrophotometer (Livingston, UK) at room temperature.

### Synthesis of 5-((pyren-4-ylmethyl) amino) pentan-1-ol (1)

1-Pyrenecarboxaldehyde (500 mg, 2.15 mmol) was dissolved in methanol (5 mL), and 5-aminopentan-1-ol (1.35 mL, 12.9 mmol) was then added. The reaction mixture was stirred under argon at room temperature for 12 h, followed by the addition of sodium triacetoxyborohydride (911 mg, 4.3 mmol), and stirred for an additional 2 h. After concentration under vacuum, the crude material was dissolved in dichloromethane and extracted with H<sub>2</sub>O three times. The organic layer was dried with anhydrous MgSO<sub>4</sub>. After removal of the solvent, flash column chromatography (silica gel; MeOH/CH<sub>2</sub>Cl<sub>2</sub>; 5:100, v/v) of the residue yielded compound **1** (348 mg, 51%) as a light-yellow solid. <sup>1</sup>H NMR (500 MHz, CDCl<sub>3</sub>) δ 8.36 (d, J = 9.2 Hz, 1H), 8.24 – 8.08 (m, 4H), 8.01 (s, 2H), 7.82-7.52 (m, 2H), 4.50 (s, 2H), 3.63 (t, J<sub>1</sub> = 6.4 Hz, J<sub>2</sub> = 6.4 Hz, 2H), 2.82 (s, 2H), 1.74-1.54 (m, 2H), 1.49-1.33 (m, 2H), 1.33-0.83 (m, 2H). <sup>13</sup>C NMR (126 MHz, CDCl<sub>3</sub>), δ 133.74, 131.31, 130.82, 130.66, 129.00, 127.66, 127.44, 127.06, 127.00, 125.87, 125.09, 124.69, 123.03, 77.30, 33.05, 26.79, 26.57, 21.72, 19.74, 15.46, 11.66, 7.44 ppm. HRMS (M<sup>+</sup>+1) found, 318.1864; calculated for C<sub>22</sub>H<sub>24</sub>NO, 318.1852.

**Synthesis of 5-hydroxy-N-(pyren-4-ylmethyl) pentan-1-aminium**

**hexafluorophosphates (V) (2)**

Compound **1** (50 mg, 0.158 mmol) was dissolved in EtOH (5 mL). Hydrogen chloride prepared using concentrated sulfuric acid and sodium chloride was passed through the solution for 10 min. After removal of the solvent under vacuum, the crude mixture was then suspended in CH<sub>2</sub>Cl<sub>2</sub> (10 mL) followed by the addition of saturated NH<sub>4</sub>PF<sub>6</sub> solution (0.75 mL) and was stirred for an additional 3h until the suspension became clear. After concentration under vacuum, the crude material was redissolved in CH<sub>2</sub>Cl<sub>2</sub> and washed with H<sub>2</sub>O. The organic phase was dried with MgSO<sub>4</sub> and then concentrated under vacuum to afford compound **2** as a yellow solid. (73.1 mg, 100%). <sup>1</sup>H NMR (CDCl<sub>3</sub>): δ 8.32 (d, J = 9.2 Hz, 1H), 8.18-8.10 (m, 4H), 8.02 (s, 2H), 8.00-7.97 (m, 2H), 4.45 (s, 2H), 3.60-3.56 (t, J<sub>1</sub> = 6.4 Hz, J<sub>2</sub> = 6.4Hz, 2H), 2.79-2.75 (t, J<sub>1</sub> = 7 Hz, J<sub>2</sub> = 7.05 Hz, 2H), 1.95 (s, 2H), 1.39 (m, 2H), 1.27 (s, 2H). HRMS found (M<sup>+</sup>-PF<sub>6</sub>), 318.1867; calculated for C<sub>22</sub>H<sub>24</sub>NO, 318.1852; HRMS found (M<sup>-</sup>), 144.9647; calculated for PF<sub>6</sub><sup>-</sup>, 144.9647.

**Synthesis of N-(9-(2-(chlorocarbonyl) phenyl)-6-(diethyl amino)-3H-xanthen-3-ylidene)-N-ethylethanaminium chloride (3)**

Rhodamine B (100 mg, 0.225 mmol) was suspended in SOCl<sub>2</sub> (5 mL), and 100 μL of DMF was added. The reaction mixture was refluxed under argon for 3h and then cooled to room temperature. Removal of solvent under vacuum afforded compound **3** (105 mg) as an intermediate reagent.

**Synthesis of RhBPy [2]rotaxane (4)**

Compound **2** (30 mg, 0.065 mmol) was dissolved in CHCl<sub>3</sub> (3 mL), and

dibenzo-24-crown-8 (58 mg, 0.13 mmol) was added. The reaction mixture was vigorously stirred in an ice-salt bath for 1h, followed by the addition of a solution of compound **3** (105 mg) in CHCl<sub>3</sub> (2 mL), and stirred for additional 2h. Three milliliters of H<sub>2</sub>O was then added into the reaction mixture and stirred for an additional 1h. The crude mixture was then extracted with CHCl<sub>3</sub>. The organic layer was dried with MgSO<sub>4</sub> and concentrated under vacuum. Chromatography of the residue on a silica gel column eluted with CH<sub>2</sub>Cl<sub>2</sub> yielded compound **4** as a red solid (12 mg, 0.0087 mmol, 16% yield). <sup>1</sup>H NMR (CDCl<sub>3</sub>): δ 8.04 (d, J = 7.6 Hz, 3H), 7.81-7.68 (m, 5H), 7.68-7.51 (m, 4H), 7.55-7.51 (m, 1H), 7.24-7.14 (m, 4H), 6.98- 6.88 (d, J = 8.75 Hz, 3H), 6.81-6.78 (d, J = 8.7 Hz, 3H), 6.67-6.58 (m, 5H), 4.33-4.29 (t, J<sub>1</sub> = 6.75 Hz, J<sub>2</sub> = 6.65 Hz, 2H), 4.10-4.18 (d, J = 6.8 Hz, 2H), 3.63-3.52 (m, 8H), 3.37-3.12 (m, 16H), 2.10-2.01 (m, 2H), 1.80-1.65 (m, 6H), 1.27 (m, 8H), 1.10-1.03 (t, J<sub>1</sub> = 7 Hz, J<sub>2</sub> = 7.05 Hz, 12H) ppm. <sup>13</sup>C NMR (CDCl<sub>3</sub>): δ 168.57, 148.30, 147.99, 145.81, 135.51, 134.44, 132.38, 130.88, 130.50, 128.83, 126.29, 125.99, 125.58, 123.82, 119.09, 117.56, 115.76, 65.54, 46.97, 39.35, 37.38, 37.08, 34.41, 32.74, 31.90, 30.55, 30.00, 29.66, 29.33, 27.95, 27.70, 27.06, 26.71, 24.44, 22.66, 19.70, 19.13, 14.07, 13.68, 13.40 ppm. HRMS [M-PF<sub>6</sub>-H+Na]<sup>+</sup> found 1248.5723; calculated for C<sub>74</sub>H<sub>84</sub>N<sub>3</sub>O<sub>11</sub>NaCl, 1248.5692.

### Fluorescence spectrum studies

A stock solution of **RhBP**y [2]rotaxane (1 mM) in CHCl<sub>3</sub> was prepared. Working solutions of **RhBP**y [2]rotaxane were freshly prepared by diluting the highly concentrated stock solution to the desired concentration prior to spectroscopic

measurements. In the fluorescence experiment, a 10  $\mu\text{M}$  (3 mL) solution of the **RhBPy** [2]rotaxane in  $\text{CHCl}_3$  was placed in a quartz optical cell with a 1-cm optical path length. Spectral data were recorded 5 min after the addition of the sample. Excitation was provided at 276 nm, and emission spectra were collected from 300 to 600 nm.

### Cell Culture

HeLa cells, MRC-5 cells and MCF-7/ADR cells were cultured with RPMI-1640 medium containing 10% FBS, 100 U/mL penicillin and 100  $\mu\text{g/mL}$  streptomycin at 37  $^\circ\text{C}$  under a 5%  $\text{CO}_2$  atmosphere. The cell culture medium was changed every 48 h. Then, HeLa cells or MCF-7/ADR cells were seeded into 24-well plates or 96-well plates at an initial cell density of  $2 \times 10^4$  cells per  $\text{cm}^2$ . When cell confluence reached approximately 70%, the culture medium was replaced with fresh medium containing samples of **RhBPy** [2]rotaxane, doxorubicin (DOX), and **RhBPy** [2]rotaxane/DOX for the following studies.

### Cellular uptake study

For fluorescence microscopy study, one day before imaging, HeLa cells were seeded in 24-well plates and incubated for 24 h. The next day, the culture medium was replaced with serum-free medium containing the **RhBPy** [2]rotaxane, and the cells were incubated at 37  $^\circ\text{C}$  for 1 h, followed by incubation of fluorescein or DOX for another predetermined period. After the treatment, the cells were rinsed three times with PBS, and fluorescence imaging of the intracellular contents was directly performed using an Olympus inverted fluorescence microscope with a magnification

of 2000× or 3200×. Cells incubated with DMSO as a solvent were adopted as a control. To further observe cell nuclei, cells were stained with Hoechst 33258 (10 µg/mL) for 5 min. Subsequently, the cells were washed with PBS three times. Cell nuclei and intracellular fluorescent **RhBPy** [2]rotaxane were directly visualized on a confocal laser scanning microscope (Olympus FLUOVIEW FV1000) under a magnification of 3200×.

### Evaluation of cytotoxicity of rotaxane and rotaxane/DOX

The cytotoxicity of **RhBPy** [2]rotaxane was evaluated in MRC-5 cells using an MTT assay. Cells were seeded into 96-well plates and cultured for 24 h. Then, the medium was replaced with 100 µL of fresh medium containing different concentrations of the **RhBPy** [2]rotaxane, and the cells were further incubated at 37 °C for an additional 24 h. Cell viability was evaluated by incubating with 0.5 mg/mL MTT for 4 h under 5% CO<sub>2</sub>/95% air at 37 °C. Media were replaced with 100 µL DMSO, and absorbance was measured at 570 nm using a plate reader (Bio-Rad 550).

To evaluate the cell inhibition efficiency of DOX and **RhBPy** [2]rotaxane/DOX, HeLa cells or MCF-7/ADR cells were directly seeded in 96-well plates and incubated at 37 °C for 24 h. The culture medium was then removed. Different concentrations of DOX or **RhBPy** [2]rotaxane/DOX were dispersed in 100 µL of culture medium and then added to each well. After the cells were incubated with DOX or **RhBPy** [2]rotaxane/DOX at 37 °C for 48 h, the cell viability was measured by an MTT assay as previously described. In addition, after MTT incubation for 30 min, phase-contrast

images were obtained using an Olympus inverted fluorescence microscopy under 1000× magnification.

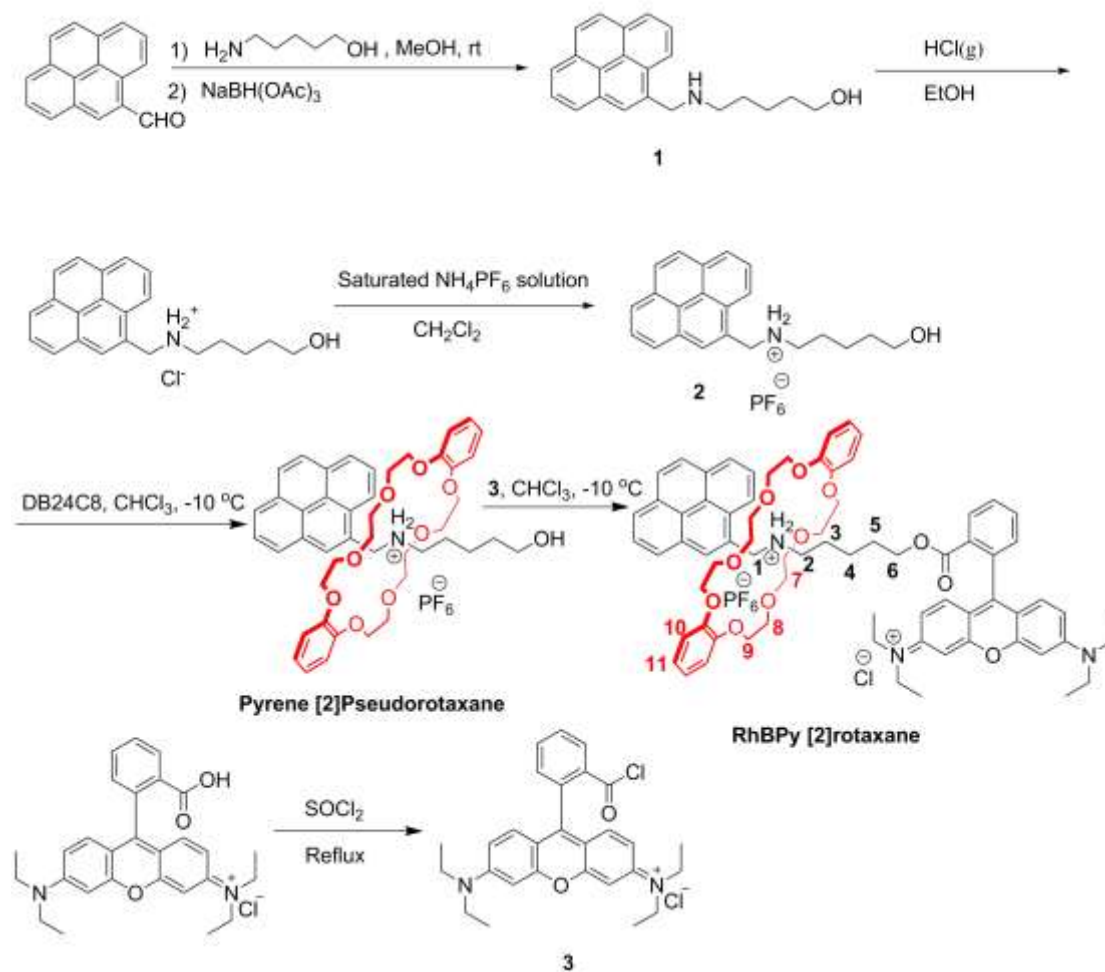
### Statistical analysis

All data were reported as means  $\pm$  standard deviation (SD). The results were compared using one-way ANOVA followed by a Bonferroni post test, and differences were considered to be significant when the *P* value was less than 0.05.

## Results and Discussion

### Synthesis of the RhBPY [2]rotaxane

The synthesis of the **RhBPY** [2]rotaxane is illustrated in **Scheme 1**. Compound **1** was obtained in 51% yield by reacting 5-aminopentan-1-ol with commercially available 1-pyrenecarboxaldehyde in MeOH at room temperature for 12 h, followed by the reduction of the imine intermediate with sodium triacetoxyborohydride. Treating **1** with HCl gas for 10 min, followed by anion exchange with saturated  $\text{NH}_4\text{PF}_6$  solution, afforded compound **2** in 100% yield. Compound **3** was prepared by refluxing Rhodamine B in  $\text{SOCl}_2$  in the presence of DMF. The targeted **RhBPY** [2]rotaxane was then obtained in 16% yield by the esterification of **3** with a pyrene [2]pseudorotaxane intermediate, which was prepared by the reaction of **2** with DB24C8 at  $-10\text{ }^\circ\text{C}$  in  $\text{CHCl}_3$ . The structure of the **RhBPY** [2]rotaxane was confirmed by  $^1\text{H}$  NMR,  $^{13}\text{C}$  NMR and HRMS (**supporting materials**).

**Scheme 1.** Synthesis of the rhodamine B pyrene [2]rotaxane

Initially, the  $^1\text{H}$  NMR spectra of the targeted **RhBPy** [2]rotaxane (**Figure 2c**) containing a dibenzene-24-crown-8 (DB24C8) ring interlocked onto a dumbbell-shaped thread with a pyrene and a Rhodamine B as two bulky fluorescent stoppers on its ends was studied by a comparison of the  $^1\text{H}$  NMR spectra with the thread **2** (**Figure 2b**) and DB24C8. As indicated in **Figure 2**, distinct downfield shifts were observed on the protons of the pyrene units ( $\Delta\delta = 0.28, 0.51$  and  $0.32$  ppm, respectively). The peaks of the protons for the thread, ( $\text{H}_1, \text{H}_2, \text{H}_3, \text{H}_4, \text{H}_5$  and  $\text{H}_6$ ) also changed tremendously ( $\Delta\delta = 0.15, -0.44, -0.16, -0.33, -0.18$  and  $-0.49$  ppm, ) due to the introduction of the Rhodamine B and the macrocycle DB24C8, which could be

ascribed to a combination of [C-H...O] and [N-H...O], the hydrogen bonding between the ammonium group, and the crown ether. These findings also directly indicated the formation of a stable mechanically interlocked structure between DB24C8 and the dumbbell-shaped 'axle'. Moreover, protons for H<sub>7</sub>, H<sub>8</sub> and H<sub>9</sub> of the macrocyclic ring produced signals in the spectrum of the macrocycle (**Figure 2a**) at 3.83 ppm, 3.92 ppm and 4.15 ppm, respectively, which were shifted downfield by  $\Delta\delta=0.60$  ppm, 0.69ppm and 0.55ppm, respectively, over the **RhBPy** [2]rotaxane. In addition, the peaks for H<sub>7</sub> and H<sub>8</sub> overlapped completely owing to the similar chemical environment. Above all, the changes in the chemical shifts provided sufficient evidence confirming that the macrocycle lay predominantly over the recognition site, namely, the secondary ammonium site in the **RhBPy** [2]rotaxane.

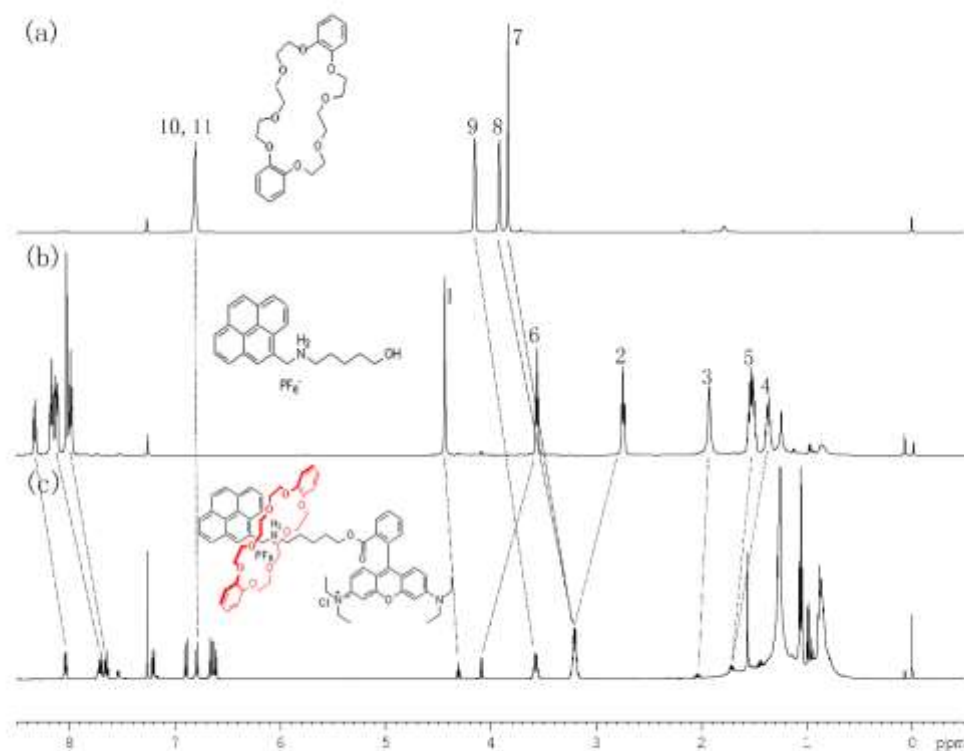


**Figure 2.** <sup>1</sup>H NMR spectra (500 MHz, CDCl<sub>3</sub>) of **a**) dibenzene-24-crown-8, **b**)

compound **2**, c) **RhBPy** [2]rotaxane.

To further investigate the interpenetrated nature of the protons of the **RhBPy** [2]rotaxane, we also acquired a NOESY NMR spectrum, which was obtained in chloroform-d. As indicated in **Figure 3**, the red point (point A) representing strong NOEs can be observed from the proton ( $H_9$ ) to positions on the benzylic proton for the pyrene ( $H_{11}$ ). Moreover, the NOESY spectrum also revealed that the proton for  $H_1$  was close to  $H_7$  and  $H_8$ . These results indicated the localization of the DB24C8 wheel at the pyrene by forming an inclusion complex with the macrocyclic cavity from head side again. All these data and the MS spectrum (**Figure 4**) of the **RhBPy** [2]rotaxane provided additional confirmation of the interlocked nature of the **RhBPy** [2]rotaxane, which indicated that the synthetic approach used in this paper was effective.

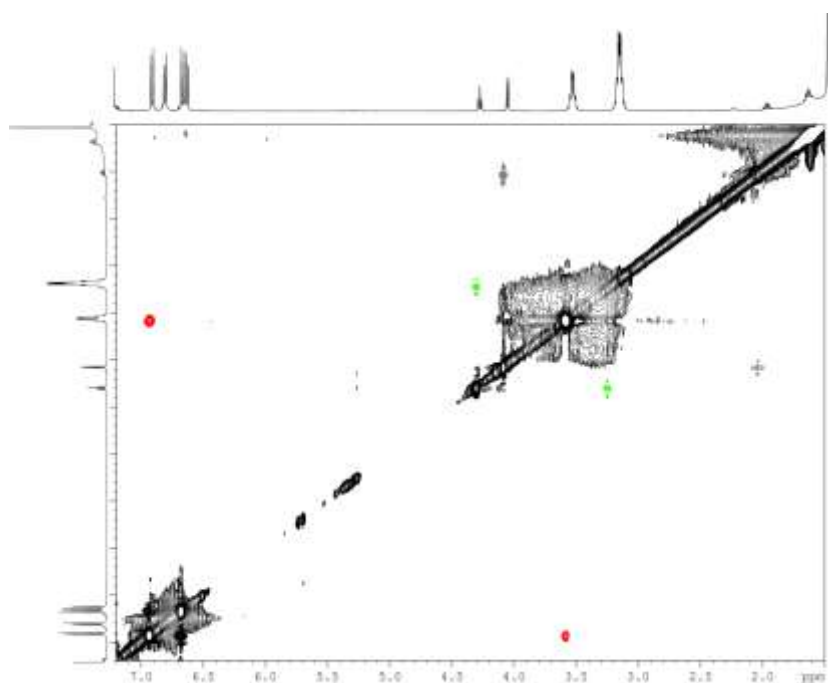


**Figure 3.** Section of the 2D NMR NOESY spectrum of the **RhBPy** [2]rotaxane in  $CDCl_3$  (500Hz)

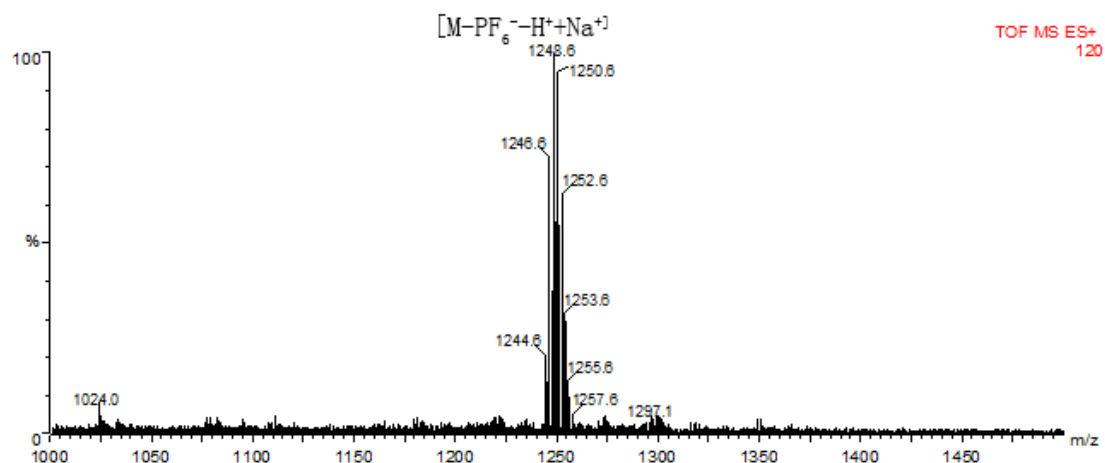


**Figure 4.** MS spectrum of the **RhBPy** [2]rotaxane.

### Thermo-driven properties of the **RhBPy** [2]rotaxane

In addition, the temperature dependence of the  $^1\text{H}$  NMR spectra of the **RhBPy** [2]rotaxane was studied from 278K to 318K to monitor the molecular switching process. **Figure 5** indicated that different temperatures did not lead to significant changes except for some changes in the chemical shift of the macrocycle and some broadening of peaks. For example, lower temperature caused marked chemical shifts of the protons for  $\text{H}_7$ ,  $\text{H}_8$  and  $\text{H}_9$  to a higher field, and there was a linear relationship between the chemical shifts of the protons for  $\text{H}_7$  ( $\text{H}_8$ ) and  $\text{H}_9$  and temperature (**Figure 6**), which was not surprising because the strength of hydrogen bonding interactions became stronger with a decrease in temperature. These data also provided convincing evidence that the movement of the ring was slow at low temperature. Apart from these changes, the peaks for  $\text{H}_7$  ( $\text{H}_8$ ) indicated a strong broadening with an increase in temperature. Likewise, the peaks assigned to  $\text{H}_{11}$ ,  $\text{H}_{12}$ ,  $\text{H}_{13}$ ,  $\text{H}_{14}$ ,  $\text{H}_{15}$ ,  $\text{H}_{16}$ ,  $\text{H}_{17}$  and  $\text{H}_{18}$  also exhibited broadening due to the increasing strength of the hydrogen bonding interaction with the macrocycle.

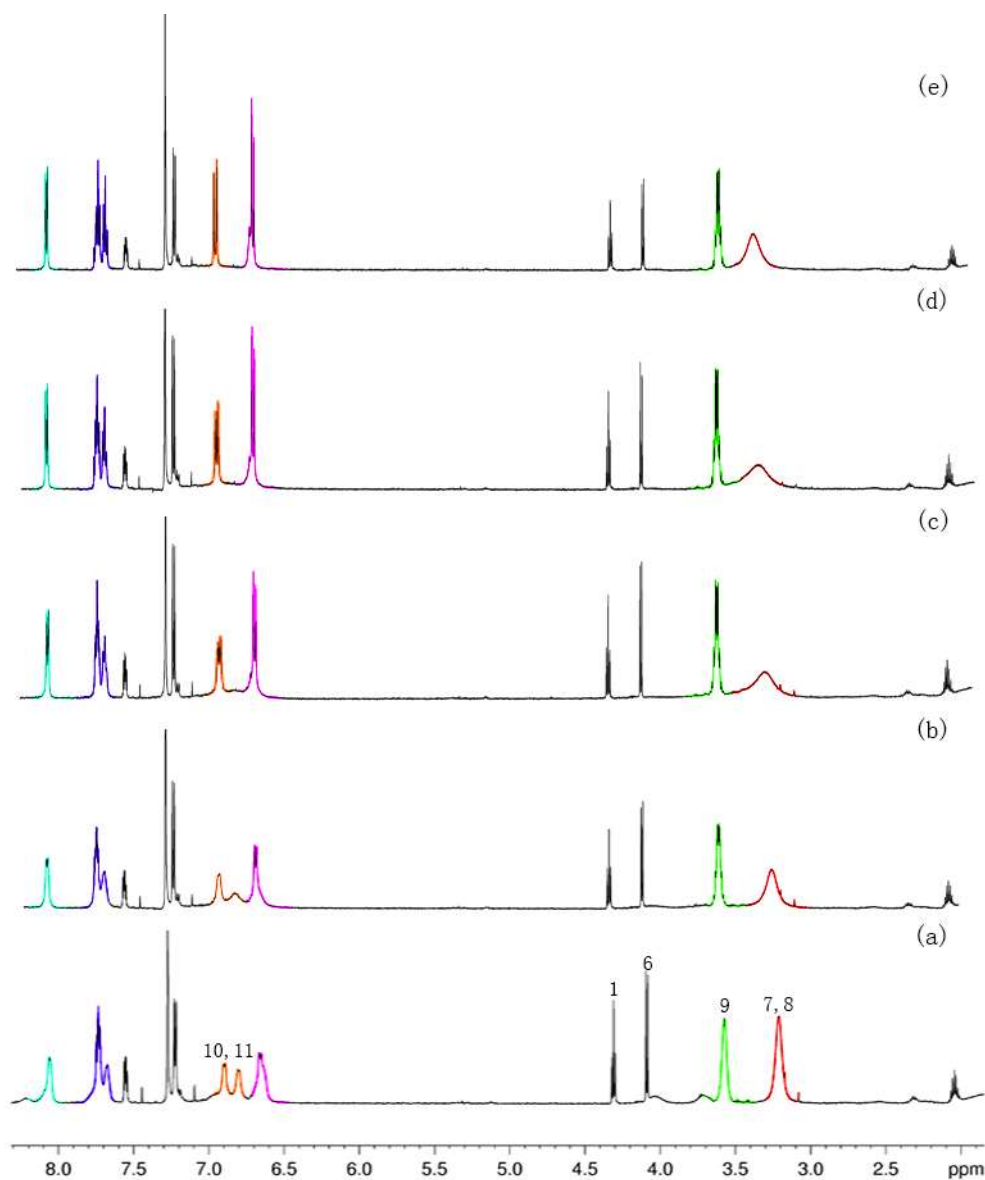


**Figure 5.** Comparison of the partial  $^1\text{H}$  NMR spectra of the RhBPy [2]rotaxane exhibiting signals from 278K to 318K.

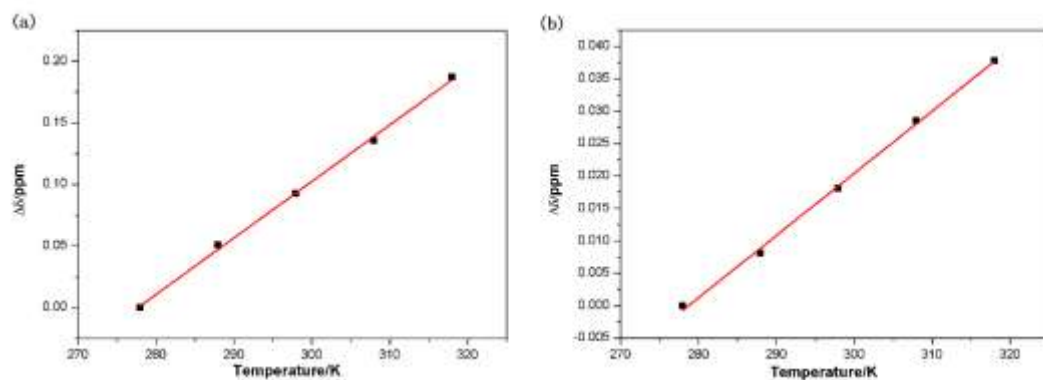


**Figure 6.** Plot of temperature vs. changes in the chemical shift of **a)** the protons of H<sub>7</sub> and H<sub>8</sub> and **b)** the protons of H<sub>9</sub>.

In marked contrast, the benzylic proton signals of the macrocycle were also compared from 278K to 318K in **Figure 5**. It can be clearly observed that the peak shape exhibited significantly different behavior. On the one hand, the H<sub>10</sub> signals coalesce simultaneously near 288K into a pair of narrow and elevated signals, which appear to coalesce completely at 298K to yield only one singlet peak. On the other hand, the shape of this signal (H<sub>10</sub>) becomes narrow and sharp with the increase in temperature above 298K. This behavior may be due to the simple fact that the rolling speed of the DB24C8 ring around the thread is restricted at low temperature, which makes the chemical environment of the protons for H<sub>10</sub> and H<sub>11</sub> different. In summary, we can control the migration of the DB24C8 ring by varying the temperature (input signals), and the changes in the chemical shift can be considered the output signals. These findings also provide additional evidence that the **RhBP**y [2]rotaxane can be applied as molecular switches that are responsive to temperature.

To establish the rate of movement of the macrocycle, kinetic parameters calculated based on the coalescence temperature of the <sup>1</sup>H NMR spectra for the dynamic process could be obtained, as shown in **Table 1**<sup>[44-45]</sup>. Based on all of these data, we concluded that the ring, driven by entropy at high temperature, moved through the axis between the two bulky stoppers. However, this change occurred without chemical reaction, and the lack of changes in the covalent structure also suggest that the compound can be used for important applications as a molecular switch.

**Table 1.** Kinetic and thermodynamic parameters of protons for H<sub>10</sub> for the movement of DB24C8 between the two bulky stoppers in the **RhBPy** [2]rotaxane at the coalescence temperature (T<sub>c</sub>=298K).

$\Delta\nu$ (Hz)	$k$ (s <sup>-1</sup> )	$\Delta G^{\circ}$ (kJ/mol)	$\Delta H$ (kJ/mol)	$\Delta S$ (J/(mol•K))
150	333.22	58.60	24.93	-112.64

### Photo-driven properties of the **RhBPy** [2]rotaxane

Next, we focused on the photo-physical properties of the **RhBPy** [2]rotaxane. First, some attempts were made to study the location of the macrocycle around the thread by fluorescence spectroscopy in CHCl<sub>3</sub>. Certain spectral changes of the **RhBPy** [2]rotaxane can be observed in the fluorescence spectra. As indicated in **Figure 7**, two strong emission signals of the **RhBPy** [2]rotaxane were observed at approximately 380 nm and 552 nm. As is well known, the emission peak for the wavelength of approximately 380 nm is ascribed to the pyrene unit, whereas the peak of the Rhodamine B unit appears at a wavelength of 552 nm, whose intensity is higher than that of the pyrene unit due to the ring-opened ester of the **RhBPy** [2]rotaxane. Moreover, highly remarkable fluorescence changes were obtained in the spectrum of the **RhBPy** [2]rotaxane in response to TEA. When 2 equivalents of TEA were added to the solution, the emission intensity of the Rhodamine B moiety decreased by 37.1% ( $\lambda_{em}=552\text{nm}$ , respectively) relative to the fluorescence intensity of the **RhBPy** [2]rotaxane. Furthermore, the fluorescence intensity of the pyrene unit showed a remarkable decrease (approximately 38%). This phenomenon can also be attributed to

the movement of the DB24C8 macrocycle upon the addition of TEA under irradiation. This behavior is based on the procedure used to synthesize the **RhBPy** [2]rotaxane, through which we can confirm that the original state of the DB24C8 resides near the recognition site of the thread. With the addition of TEA, the hydrogen bonding interaction was weakened between the recognition sites and the macrocycle, which led to the migration of the DB24C8 ring in the **RhBPy** [2]rotaxane under irradiation. In other words, the DB24C8 ring shifted toward the Rhodamine B moiety when TEA was added.

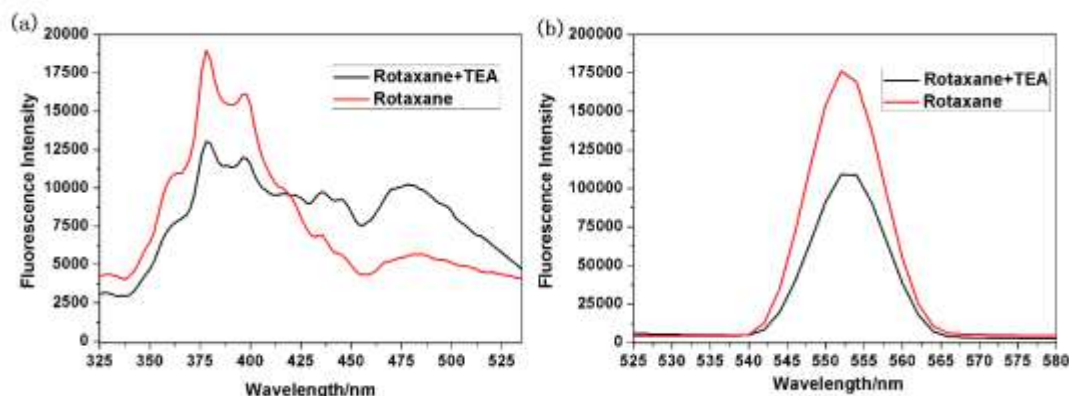


**Figure 7.** Changes in the fluorescence spectrum of the **RhBPy** [2]rotaxane ( $10\mu\text{M}$ ) in  $\text{CHCl}_3$  and in the spectrum of the mixture obtained after adding 2 equivalents of triethylamine (TEA) to the rotaxane solution.

In addition, as the DB24C8 ring shifted away from the pyrene unit toward the Rhodamine B unit, the fluorescence intensity of the **RhBPy** [2]rotaxane changed significantly, which also indicates that the DB24C8 ring could quench the fluorescence of the Rhodamine B moiety. This phenomenon indicates that the DB24C8 ring shows distinct fluorescence quenching characteristics. The reason

appears to be that the weak electrostatic interaction makes the electron cloud density change between Rhodamine B and DB24C8, which may result in the fluorescence quenching of the former. Moreover, based on the fluorescence spectrum of the **RhBPy** [2]rotaxane, we conclude that the **RhBPy** [2]rotaxane shows strong fluorescence, which also indicates that we can monitor the cellular permeability of the rotaxane during the transport process and determine its cellular location in HeLa cells during the course of drug delivery by fluorescence microscopy.

### Cellular uptake of **RhBPy** [2]rotaxane

Previous studies have not determined the exact cellular localization of the rotaxane after its incubation in cells<sup>[38-39]</sup>. To investigate the cellular uptake and localization of the new rhodamine-conjugated rotaxane, studies were carried out to assess the fluorescence imaging of the **RhBPy** [2]rotaxane. The uptake of the **RhBPy** [2]rotaxane by HeLa cells was studied. Because rotaxane conjugated with Rhodamine B is fluorescent, it can be directly observed by fluorescence microscopy. As demonstrated by the fluorescence microscopy images displayed in **Figure 8**, significant red fluorescence appeared when HeLa cells were incubated with 5  $\mu\text{M}$  or 10  $\mu\text{M}$  of the **RhBPy** [2]rotaxane at 37  $^{\circ}\text{C}$  for 1 h (**Figure 8**). These results indicate that the **RhBPy** [2]rotaxane is capable of penetrating into cells and that the cellular uptake of the **RhBPy** [2]rotaxane increases with the increase in the rotaxane concentration.

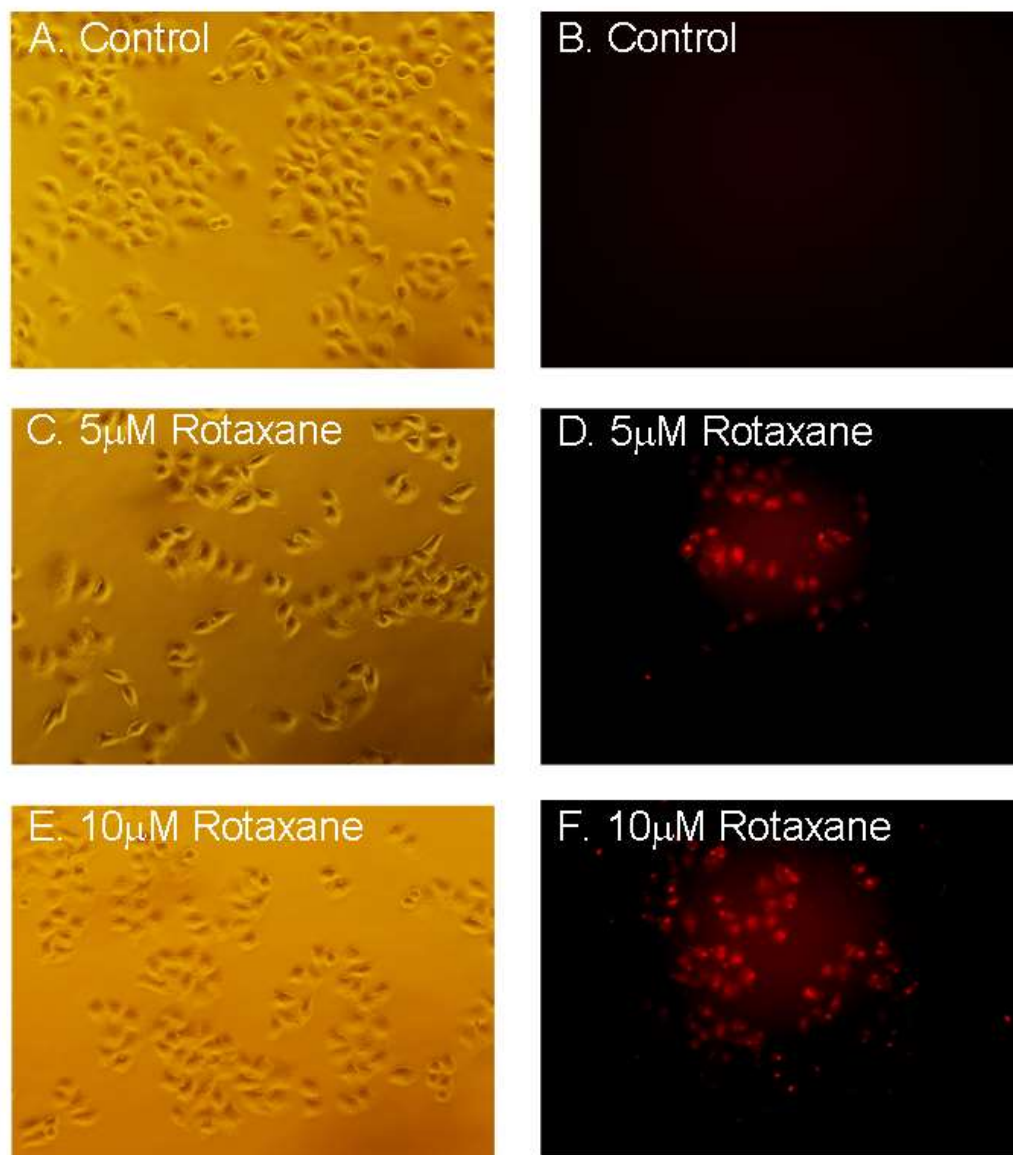


**Figure 8.** Fluorescence microscopy images of HeLa cells incubated with the **RhBPy** [2]rotaxane. The cells were incubated with 5  $\mu\text{M}$  or 10  $\mu\text{M}$  of the **RhBPy** [2]rotaxane(Rotaxane) for 1 h and were then observed under a microscope for fluorescence (left panels: white light; right panels: **RhBPy** [2]rotaxane fluorescence).

To further evaluate the intracellular localization of the **RhBPy** [2]rotaxane, the HeLa cells were grown on microscope slides. The cells were exposed to the **RhBPy** [2]rotaxane (5  $\mu\text{M}$ ) in serum-free medium for 1 h at 37  $^{\circ}\text{C}$ . Cells were examined by a confocal laser scanning microscopy. To distinguish the intracellular cytoplasm and

nucleus, the cells were stained with Hoechst 33528 to observe the blue fluorescence of nuclei. The fluorescence microscopy images of HeLa cells under higher magnification shown in **Figure 9** indicate that the **RhBPy** [2]rotaxane was located in the cytoplasm and the nucleus of HeLa cells but was mainly distributed in the cytoplasm. These data suggest that the synthesized **RhBPy** [2]rotaxane can transport molecules into cells, which was demonstrated in a previous study reporting the observation of fluoresceinated peptides in the cellular cytoplasm and nucleus when COS-7 cells were exposed to rotaxane and fluoresceinated peptides <sup>[39]</sup>.

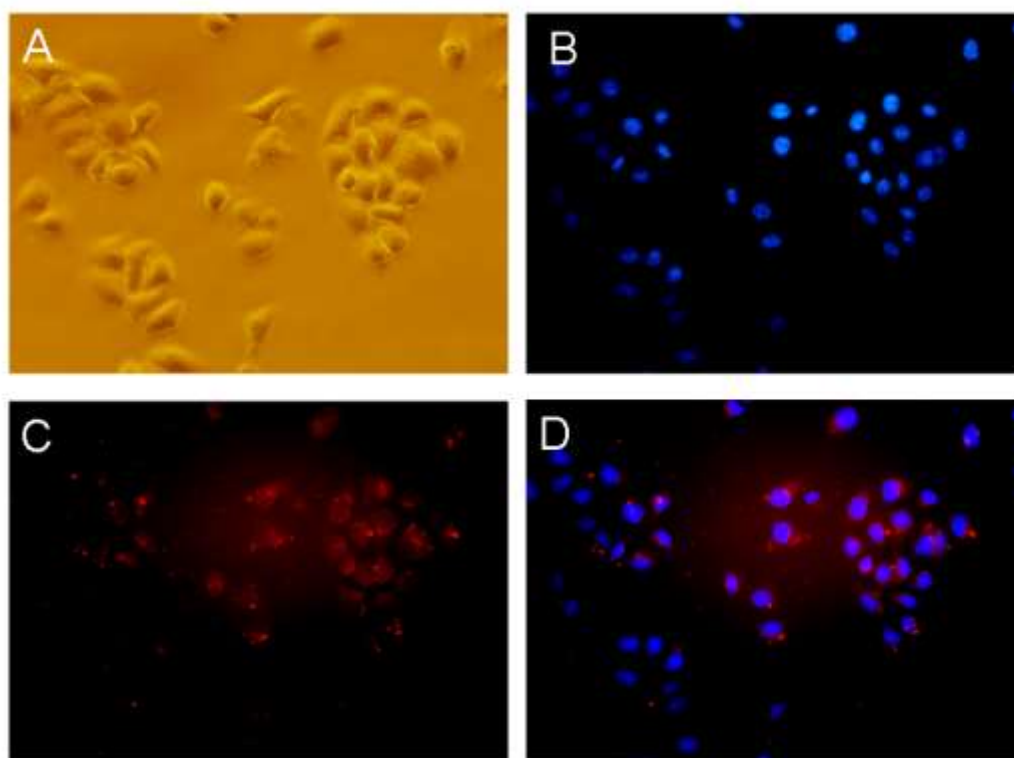


**Figure 9.** Fluorescence photomicrographs showing one representative example of HeLa cells exposed to the **RhBPy** [2]rotaxane. The cells were incubated with 5  $\mu\text{M}$  of the **RhBPy** [2]rotaxane for 1 h and then were observed under a confocal laser scanning microscope for fluorescence (A, white light; B, cell nuclei stained with Hoechst 33258; C, fluorescence of the **RhBPy** [2]rotaxane; D, merging of the images

shown in B and C).

To test the cellular transport efficiency of the newly synthesized **RhBPy** [2]rotaxane, we determined the compound's ability to transport fluorescein into HeLa cells. Fluorescein was chosen as the guest to investigate the cellular transport efficiency of the **RhBPy** [2]rotaxane because its strong green fluorescence can be monitored within cells. The cells were plated on 24-well plates, placed in serum-free medium, and incubated with fluorescein (20  $\mu\text{M}$ ) or the **RhBPy** [2]rotaxane (5  $\mu\text{M}$ ) for 1 h at 37°C before fluorescein (20  $\mu\text{M}$ ) was added. After an additional two hours, the cells were washed thoroughly, and then the cellular delivery of fluorescein was visualized using fluorescence microscopy. As indicated in **Figure S10** (**Supporting Materials**), fluorescein did not noticeably penetrate the cells (**Figure S10C**, **Supporting materials**), but high and moderate fluorescence was observed in cells that were exposed to the mixtures of fluorescein (20  $\mu\text{M}$ ) and the **RhBPy** [2]rotaxane (5  $\mu\text{M}$ ). Cell viability results indicate that the mixtures of the **RhBPy** [2]rotaxane and fluorescein were not toxic to the cells (**Figure S11**, Supporting Materials).

#### **Cellular drug delivery by the RhBPy [2]rotaxane**

To further investigate the potential of the **RhBPy** [2]rotaxane as a drug delivery agent, the ability of the **RhBPy** [2]rotaxane to transport the cancer drug doxorubicin (DOX) into HeLa cells was determined. DOX specifically interacts with the DNA of tumor cells to induce apoptosis and cell death. The *in vitro* cell inhibition efficiency of DOX with the **RhBPy** [2]rotaxane was evaluated by an MTT assay and phase-contrast imaging. As indicated in **Figure 10**, the viability of MRC-5 healthy

cells after being treated with the different concentrations of the **RhBPy** [2]rotaxane did not change significantly relative to that of the untreated control, indicating that the **RhBPy** [2]rotaxane did not exhibit cytotoxicity. As shown in **Figure 11**, the growth of HeLa cells was severely inhibited after incubation with DOX and the mixtures of DOX and the **RhBPy** [2]rotaxane. The inhibition efficiency of the mixtures of DOX and the **RhBPy** [2]rotaxane with respect to the growth of HeLa cells was higher than that of DOX alone over 48 h. DOX dose-dependently inhibited cell growth with an  $IC_{50}$  value of  $0.4 \mu\text{M}$ , but co-incubation of DOX and the **RhBPy** [2]rotaxane could inhibit cell growth more efficiently, demonstrating a three-fold lower  $IC_{50}$  value of  $0.13 \mu\text{M}$  compared to the value measured for DOX alone. In addition, co-incubation of  $0.5 \mu\text{M}$  DOX and the **RhBPy** [2]rotaxane ( $5 \mu\text{M}$ ) exhibited the highest rate of cell death, as indicated in the phase-contrast images (**Figure 11C**). These results indicate that the **RhBPy** [2]rotaxane may efficiently deliver DOX through cellular membrane barriers into the cytoplasm and the nucleus, suggesting a high potential for inhibiting the growth of cancer cells.

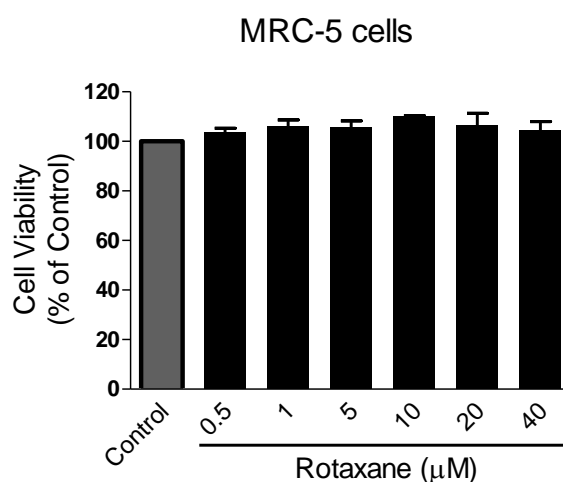
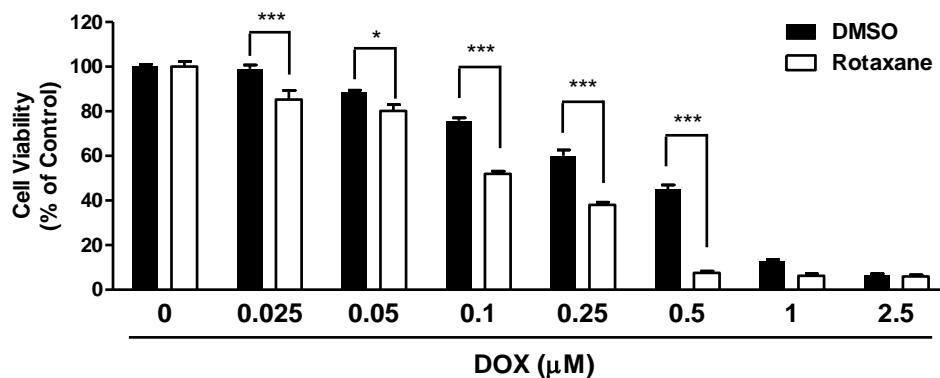


**Figure 10.** Cytotoxicity of the **RhBPy** [2]rotaxane in human fetal lung fibroblast

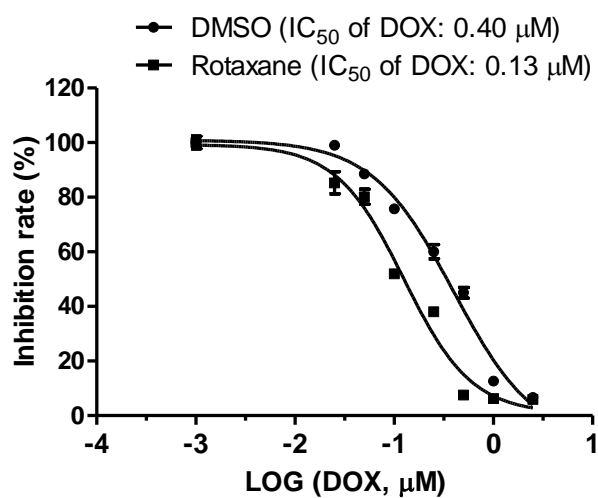
MRC-5 cells. The cells were incubated with different concentrations of the **RhBPy** [2]rotaxane(Rotaxane) for 24 h, and cell viability was determined by an MTT assay.

Data are expressed as means  $\pm$  SD.

**A.**



**B.**



**C.**

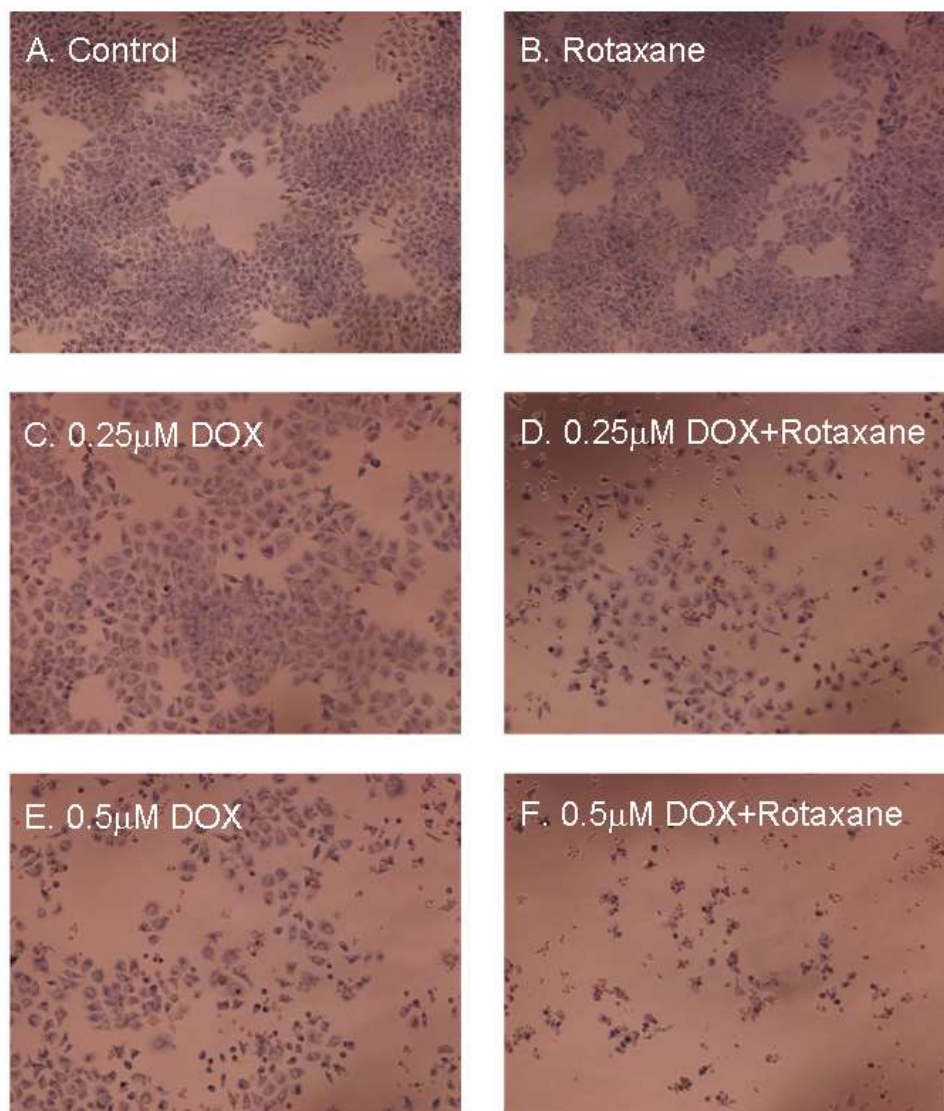


**Figure 11.** Cell viability,  $IC_{50}$  value and phase-contrast microscopy of HeLa cells after being treated with different doses of doxorubicin (DOX) and/or 5  $\mu$ M of the **RhBP**y [2]rotaxane(Rotaxane) for 48 h. Data represent means  $\pm$  SD.

To study the detailed mechanism of DOX delivery, a confocal laser scanning microscope (CLSM) was used to visualize the HeLa cells after being treated with DOX, the **RhBP**y [2]rotaxane, or mixtures of DOX and the **RhBP**y [2]rotaxane. The cells were incubated with DOX (5  $\mu$ M) for 1 h or the **RhBP**y [2]rotaxane (5  $\mu$ M) for 1 h or preincubated with the **RhBP**y [2]rotaxane (5  $\mu$ M) for 1 h followed by exposure

to DOX (5  $\mu\text{M}$ ) for an additional 1 h. Because DOX itself is fluorescent, it can be directly observed by CLSM without the use of additional labels. As depicted in **Figure 12**, the amount of DOX alone transported into the cells was limited and mainly localized in the cell nucleus, and the **RhBPy** [2]rotaxane alone was mostly transported into the cellular cytoplasm, as previously shown in **Figure 9**. However, the cells treated with DOX and the **RhBPy** [2]rotaxane together exhibited distinctly enhanced red fluorescence in the nucleus compared to the cells treated with DOX alone, suggesting enhanced DOX accumulation in the cells. Clearly, co-incubation of DOX and the **RhBPy** [2]rotaxane exhibited enhanced cellular uptake and nuclear localization of DOX compared with the single DOX treatment. The CLSM observations were consistent with the results of the MTT assay and phase-contrast imaging (**Figure 11**), indicating that co-incubation of the DOX and the **RhBPy** [2]rotaxane exhibited better cell inhibition than DOX alone. This result could be due to the different cellular uptake mechanisms of the single DOX treatment and co-incubation of DOX with the **RhBPy** [2]rotaxane. DOX alone was transported into the cells through passive diffusion across the cellular membrane, whereas DOX, when co-incubated with the **RhBPy** [2]rotaxane, entered the cells by rotaxane-mediated drug delivery. DOX was transported into the cytoplasm and nucleus by the **RhBPy** [2]rotaxane, resulting in high inhibition of cell growth. The successful transport of DOX suggests that other drugs can also be transported and thus demonstrate enhanced beneficial effects. These results indicate that cellular drug delivery could be enhanced by the **RhBPy** [2]rotaxane, which may have promising applications in improving the

therapeutic efficiency of multiple clinical drugs.

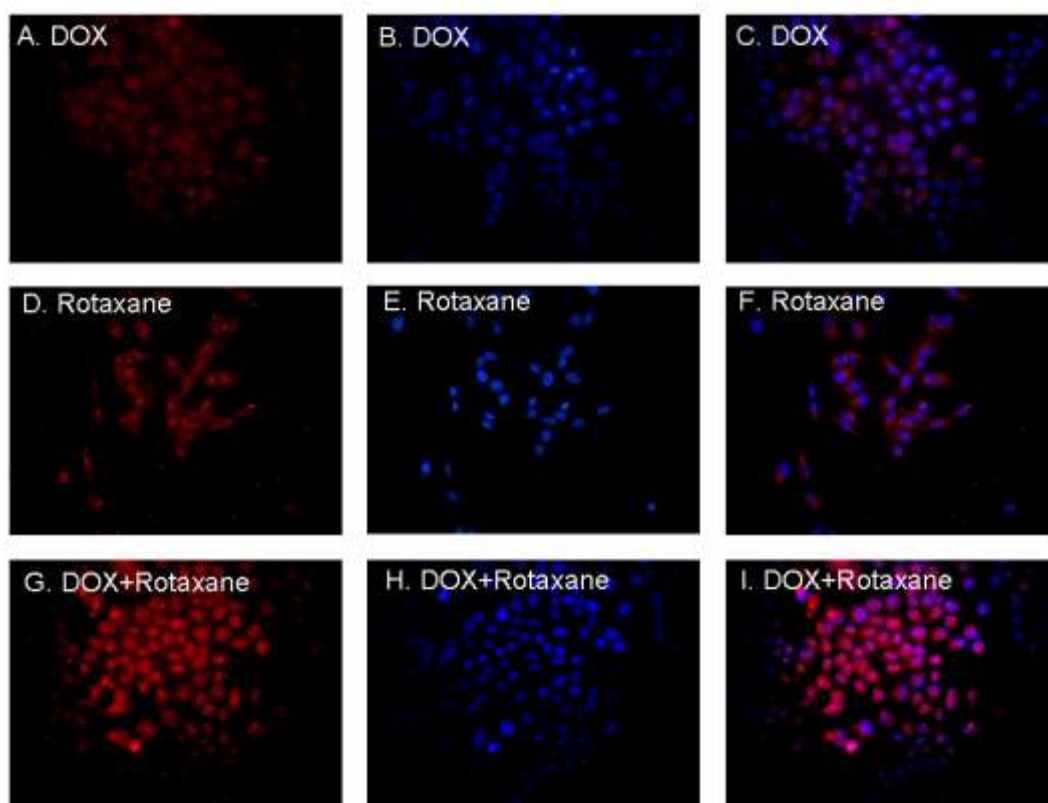
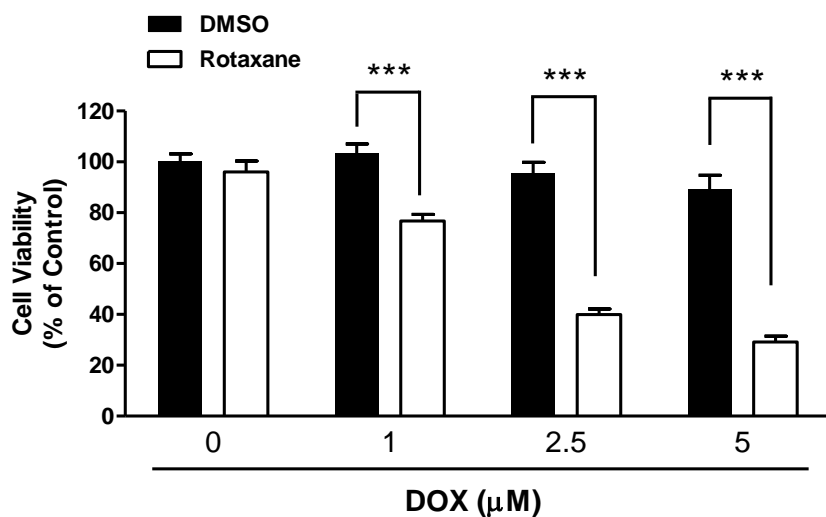


**Figure 12.** Fluorescence photomicrographs showing one representative sample of HeLa cells exposed to doxorubicin (DOX), Rotaxane, and DOX with Rotaxane. The cells were incubated with DOX (5  $\mu$ M) for 1 h, or Rotaxane (5  $\mu$ M) for 1 h, or preincubated with Rotaxane (5  $\mu$ M) for 1 h followed by exposure to DOX (5  $\mu$ M) for another 1 h, and then were observed under a confocal laser scanning microscope for fluorescence. Representative pictures are shown (A, D, G: fluorescence emission of DOX or Rotaxane; B, E, H: cell nuclei stained with Hoechst 33258; C, F, I: the merged fluorescence images).

**A.**



**B.**

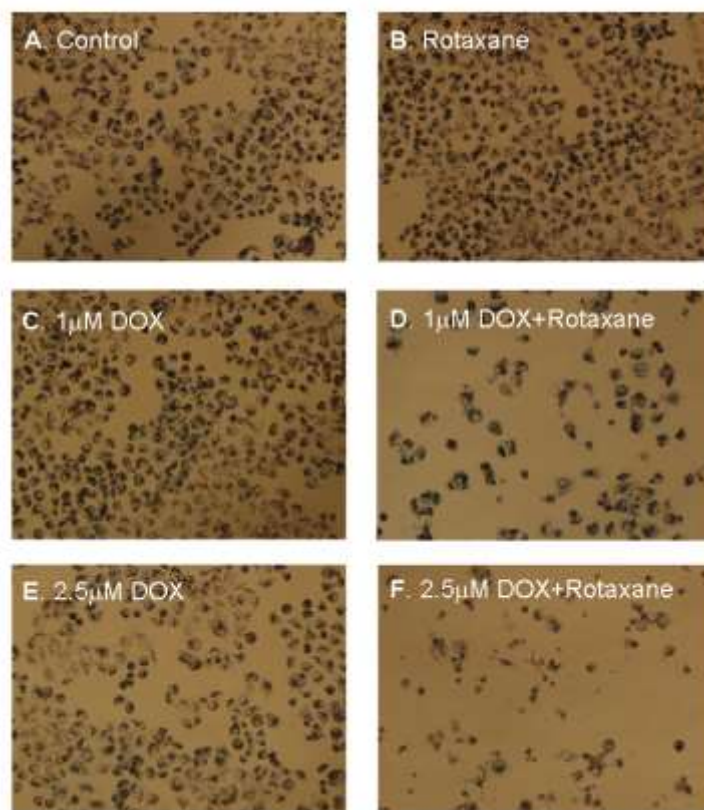


**Figure 13.** Cell viability and phase-contrast microscopy of MCF-7/ADR cells (drug-resistance human breast cancer cells) after being treated by different doses of doxorubicin (DOX) and/or 5  $\mu\text{M}$  Rotaxane for 48 h. Data represent means  $\pm$  SD.

In order to further study the drug delivery role of **RhBP**y [2]rotaxane in different

mechanism, we determined the DOX drug delivery by rotaxane in DOX-resistance MCF-7/ADR cells (drug-resistance human breast cancer cell)<sup>[46-47]</sup>. The results in **Figure 13** showed that the MCF-7/ADR cells are resistant to DOX-induced cell death, but combination treatment of DOX and **RhBPy** [2]rotaxane significantly reduced the cell viability of MCF-7/ADR, suggesting that the different cell entry mechanisms of the single DOX treatment and combination treatment of DOX and **RhBPy** [2]rotaxane. This data demonstrated that only DOX co-incubated with the **RhBPy** [2]rotaxane, can entered the nucleus of the drug-resistant cells by rotaxane-mediated drug delivery to cause cell death.

#### The complexation of DOX with **RhBPy** [2]rotaxane

To further understand the binding of DOX with **RhBPy** [2]rotaxane, fluorescence quenching assays were performed to obtain the association constants. MeCN was freshly distilled prior to making the stock solutions and performing the assays. The water solution was buffered with phosphate (1 mM) at pH 7.0. These MeCN and buffered water solutions were used to represent the polarities of the lipid portion of cells the aqueous domain respectively. Fluorescence titration experiments of **RhBPy** [2]rotaxane with **DOX** were first performed in a buffed water solution. The association constant was calculated by using the Benesi-Hildebrand plot  $F - F_0 = \Delta F = [\text{DOX}](F_{\text{max}} - F_0) / (1/K_a + [\text{DOX}])$  based on a 1:1 stoichiometry, where  $F$  is the obtained fluorescence intensity,  $F_0$  is the fluorescence intensity of free **RhBPy** [2]rotaxane at the emission wavelength and  $F_{\text{max}}$  is the saturated fluorescence intensity of the **RhBPy** [2]rotaxane-DOX complex. As shown in **Figure 14**, the

association constant ( $K_a$ ) was evaluated graphically by plotting  $1/[F-F_0]$  vs  $1/[DOX]$ . A linear relationship was obtained, and the binding constant was then calculated to be  $6.31 \times 10^5 \text{ M}^{-1}$  in a buffered water solution (1 mM, pH 7.0) as inferred from the fluorescence titration curves of **RhBPy** [2]rotaxane with the DOX (**Supporting materials**). The binding constant of the **RhBPy** [2]rotaxane with DOX in  $\text{CH}_3\text{CN}$  solution was also determined to be  $8.91 \times 10^4 \text{ M}^{-1}$ . The proposed complexation mechanism of **RhBPy** [2]rotaxane with the DOX was illustrated in **Scheme 2**. All these results with efficient delivery of DOX into HeLa cells and MCF-7/ADR cells suggest that the **RhBPy** [2]rotaxane forms a noncovalent complex with DOX in the different environments and carries it across the cells membrane.

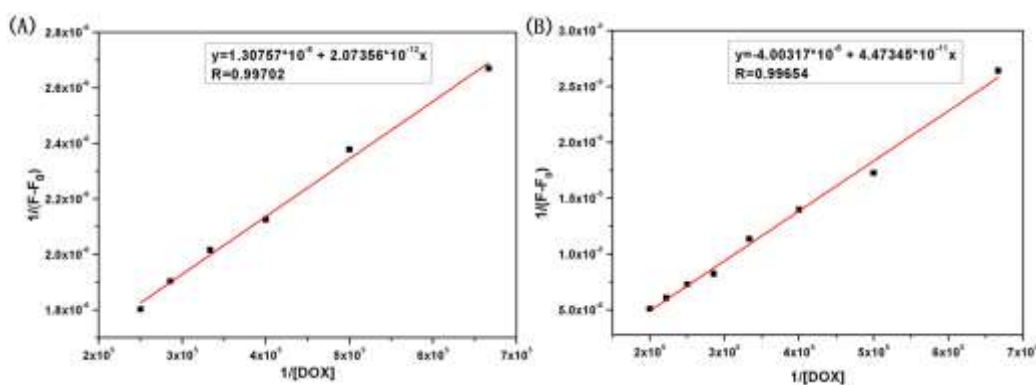
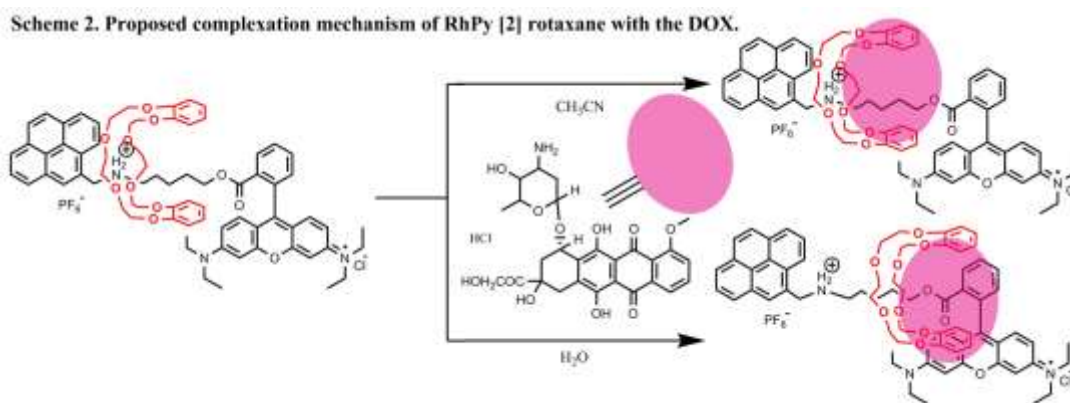


**Figure 14.** Benesi-Hildebrand plot ( $\lambda_{\text{em}} = 580 \text{ nm}$ ) of  $1/(F - F_0)$  vs.  $1/[DOX]$  in (A) buffered water solution (1 mM, pH 7.0), (B)  $\text{CH}_3\text{CN}$ .



## Conclusions

To monitor the cellular permeability of rotaxane during the transport process and determine its cellular location, a novel **RhBPy** [2]rotaxane containing a dibenzene-24-crown-8 ring interlocked onto a dumbbell-shaped thread with a pyrene stopper on its ends was designed, synthesized and structurally characterized. A comparison of the  $^1\text{H}$  NMR spectra of the **RhBPy** [2]rotaxane with those of **2** and DB24C8 provides evidence that the DB24C8 ring was successfully interlocked onto a dumbbell-shaped thread. Nuclear Overhauser effect spectroscopy (NOESY), mass spectrometry (MS) and fluorescence spectroscopy further confirmed the interlocked nature of the **RhBPy** [2]rotaxane. The temperature dependence of the rotaxane studied by  $^1\text{H}$  NMR demonstrated that the migration of the DB24C8 ring on the thread can be controlled by varying the temperature and provided additional evidence that the **RhBPy** [2]rotaxane can be applied as a molecular switch. The **RhBPy** [2]rotaxane was also demonstrated to be an efficient transport agent for delivering the cancer drug DOX into tumor cells. Indeed, DOX delivered by the **RhBPy** [2]rotaxane could effectively inhibit the growth of tumor cells. These promising results encourage us to investigate the biological response of the **RhBPy** [2]rotaxane when incorporated with different drugs, which should be helpful in developing future clinical applications.

## Acknowledgments

This research was supported by the National Natural Science Foundation of China (81371616, 21402241), Specially-appointed Professor Grant by JiangSu province

(2015, Prof. Jing Zhu), the Natural Science Foundation of Jiangsu Province (BK20130653), the Research Fund for the Doctoral Program of Higher Education of China (20133219120020).

**The authors declare no competing financial interest.**

### Notes and references

- 1 M. Xue, Y. Yang, X. Chi, X. Yan, F. Huang, *Chem. Rev.* 2015, 115, DOI:10.1021/cr5005869.
- 2 C. J. F. Rijcken, O. Soga, W. E. Hennink, C. F. Van Nostrum, *J Control Release*, 2007, 120: 131-148.
- 3 M. Prato, K. Kostarelos, A. Bianco, *Accounts Chem Res*, 2007, 41: 60-68.
- 4 G. Yu, W. Yu, Z. Mao, C. Gao, F. Huang, *Small*, 11:919-925.
- 5 G. Yu, K. Jie, F. Huang, *Chem Rev*, 2015,115,DOI: 10.1021/cr5005315.
- 6 X. Wang, D. B. Smithrud, *Bioorg Med Chem Lett*, 2011, 21: 6880-6883.
- 7 A. Gupta, P. Saha, C. Descôteaux, V. Leblanc, É. Asselin, G. Bérubé *Bioorg Med Chem Lett*, 2010, 20: 1614-1618.
- 8 C. Sánchez-Cano, M. J. Hannon, *Dalton T*, 2009 48: 10765-10773.
- 9 C Ducani, A. Leczkowska, N. J. Hodges, M. J. Hannon, *Angew Chemie*, 2010, 122: 9126-9129.
- 10 N. Salamat-Miller, M. Chittchang, T. P. Johnston, *Adv Drug Deliver Rev*, 2005, 57: 1666-1691.
- 11 Y. Yang, Y. Sun, N. Song, *Acc. Chem. Res*, 2014, 47: 1950-1960.
- 12 C. E. B. Caesar, E. K. Esbjörner, P. Lincoln, B. Nordén, *Biochemistry-US*, 2006, 45: 7682-7692.
- 13 L. Johnson, H. Mulcahy, U. Kanevets, Y. Shi, S. Lewenza, *J Bacteriol*, 2012, 194: 813-826.
- 14 W. E. Visser, E. C. Friesema, J. Jansen, T. J. Visser, *Trends Endocrin Met*, 2008, 19: 50-56.

- 15 A. D'Emanuele, D. Attwood, *Adv Drug Deliver Rev*, 2005, 57: 2147-2162.
- 16 B. K. Nanjwade, H. M. Bechra, G. K. Derkar, F. V. Manvi, V. K. Nanjwade, *Eur J Pharm Sci*, 2009, 38: 185-196.
- 17 H. Meng, M. Liong, T. Xia, Z. Li, Z. Ji, J. I. Zink, A. E. Nel, *ACS Nano*, 2010, 4: 4539-4550.
- 18 K. Yang, L. Weng, Y. Cheng, H. Zhang, J. Zhang, Q. Wu, T. Xu, *J Phy Chem B*, 2011, 115: 2185-2195.
- 19 Q. Wang, D. Qu, J. Ren, K. Chen, H. Tian, *Angew Chem Int Edit*, 2004, 43: 2661-2665.
- 20 L. Zhu, X. Li, F. Y. Ji, X. Ma, Q. Wang, H. Tian, *Langmuir*, 2009, 25: 3482-3486.
- 21 N. Song, Y. Yang. *Chem. Soc. Rev*, 2015. Doi: 10.1039/c5cs00243e.
- 22 D. Qu, Q. Wang, H. Tian, *Angew Chem Int Edit*, 2005, 44: 5296-5299.
- 23 X. Ma, D. Qu, F. Ji, Q. Wang, L. Zhu, Y. Xu, H. Tian, *Chem Commun*, 2007 14: 1409-1411.
- 24 A. Yamauchi, Y. Sakashita, K. Hirose, T. Hayashita, I. Suzuki, *Chem Commun*, 2006 41: 4312-4314.
- 25 Y. Li, L. Cao, H. Tian, *J Org Chem*, 2006, 71: 8279-8282.
- 26 X. Wang, J. Zhu, D. B. Smithrud. *J Org Chem*, 2010, 75: 3358-3370.
- 27 S. Futaki, *Adv Drug Deliver Rev*, 2005, 57: 547-558.
- 28 J. Zhu, B. E. House, E. Fleck, I. Isaacsohn, A. F. Drew, D. B. Smithrud, *Bio Med Chem Lett*, 2007, 17: 5058-5062.
- 29 Z. Zhang, C. Han, G. Yu, F. Huang, *Chem. Sci*, 2012, 3: 3026-3031.
- 30 J. Shi, X. Cao, X. Wang, X. Nie, B. Zhou, X. Bao, J. Zhu, *Tetrahedron*, 2015, 71, 4116-4123
- 31 L. Zhu, X. Ma, F. Ji, Q. Wang, H. Tian, *Chem-Eur J*, 2007, 13: 9216-9222.
- 32 C. Zhang, S. Li, J. Zhang, K. Zhu, N. Li, F. Huang, *Org. Lett*, 2007, 9: 5553-5556.
- 33 T. Ogoshi, T. Aoki, R. Shiga, R. Iizuka, S. Ueda, K. Demachi, D. Yamafuji, H. Kayama, T. A. Yamagishi, *J Am Chem Soc*, 2012, 134: 20322-20325.
- 34 C. Romuald, G. Cazals, C. Enjalbal, F. Coutrot, *Organic letters*, 2012, 15: 184-187.
- 35 V. Blanco, A. Carlone, K. D. Hänni, D. A. Leigh, B. Lewandowski, *Angew Chem*,

- 2012, 124: 5256-5259.
- 36 Jr. J. D. Megiatto, D. I. Schuster, G. de Miguel, S. Wolfrum, D. M. Guldi, *Chem Mater*, 2012, 24: 2472-2485.
- 37 Y. Kohsaka, K. Nakazono, Y. Koyama, S. Asai, T. Takata, *Angew Chem Int Edit*, 2011, 50: 4872-4875.
- 38 X. Wang, X. Bao, M. McFarland-Mancini, I. Isaacsohn, A. F. Drew, D. B. Smithrud, *J Am Chem Soc*, 2007, 129: 7284-7293.
- 39 X. Bao, I. Isaacsohn, A. F. Drew, D. B. Smithrud, *J Am Chem Soc*, 2006, 128: 12229-12238.
- 40 X. Bao, X. Cao, X. Nie, Y. Xu, W. Guo, B. Zhou, L. Zhang, H. Liao, T. Pang, *Sensor Actuat B-Chem*, 2015, 208: 54-66.
- 41 D. Liu, T. Pang, K. Ma, W. Jiang, X. Bao, *RSC Adv*, 2014, 4: 2563-2567.
- 42 X. Bao, X. Cao, X. Nie, Y. Jin, B. Zhou, *Molecules* 2014, 19: 7817-7831.
- 43 X. Bao, J. Shi, X. Nie, B. Zhou, X. Wang, L. Zhang, H. Liao, T. Pang, *Bioorg Med Chem*, 2014, 22: 4826-4835.
- 44 S. Jayasundera, W. F. Schmidt, C. J. Hapeman, A. Torrents, *J Agr Food Chem*, 1999, 47: 4435-4442.
- 45 D. D. Günbas, A. M. Brouwer, *J Org Chem*, 2012, 77: 5724-5735.
- 46 F. Peng, Y. Su, X. Ji, Y. Zhong, X. Wei, Y. He, *Biomaterials*, 2014, 35: 5188-5195.
- 47 Q. Li, Y. Sun, Y. Sun, J. Wen, Y. Zhou, Q. Bing, L. D. Isaacs, Y. Jin, H. Gao, Y. Yang, *Chem. Mater*, 2014, 26(22): 6418-6431.